Advanced Powder Technology 31 (2020) 464–476

Contents lists available at ScienceDirect

Advanced Powder Technology

journal homepage: www.elsevier.com/locate/apt

Original Research Paper

Selective catalytic reduction of NO_x by CO (CO-SCR) over metal-supported nanoparticles dispersed on porous alumina ☆

Lais F. Oton [a], Alcineia C. Oliveira [a], Jesuina C.S. de Araujo [b], Rinaldo S. Araujo [c], Francisco F. de Sousa [d], Gilberto D. Saraiva [e], Rossano Lang [f], Larissa Otubo [g], Gian Carlos da Silva Duarte [h], Adriana Campos [h]

[a] Universidade Federal do Ceará, Campus do Pici-Bloco 940, Departamento de Química Analítica e Físico-Química, Fortaleza, Ceará, Brazil
[b] Universidade Federal do Espírito Santo, Centro Universitário Norte do Espírito Santo, São Mateus, Espírito Santo, Brazil
[c] Instituto Federal de Educação – IFCE, Campus de Fortaleza, Av. 13 de Maio, 2081, Benfica, C.P. 60040-531 Fortaleza, Ceará, Brazil
[d] Universidade Federal do Pará, R. Augusto Corrêa, 1 – Guamá, Belém, 66075-110 Para, Brazil
[e] Faculdade de Educação Ciências e Letras do Sertão Central, Universidade Estadual do Ceará, Quixadá, Brazil
[f] Centro de Ciência e Tecnologia de Materiais – CCTM, Instituto de Pesquisas Energéticas e Nucleares – IPEN, 05508-000 São Paulo, São Paulo, Brazil
[g] Instituto de Ciência e Tecnologia – ICT, Universidade Federal de São Paulo – UNIFESP, 12231-280 São José dos Campos, SP, Brazil
[h] Centro de Tecnologias Estratégicas do Nordeste, CETENE, Av. Prof. Luís Freire, 1 – Cidade Universitária, Recife, PE 50740-545, Brazil

ARTICLE INFO

Article history:
Received 14 June 2019
Received in revised form 25 October 2019
Accepted 6 November 2019
Available online 18 November 2019

Keywords:
Al_2O_3
Nanoparticles
Support
Catalysts
SCR

ABSTRACT

The selective catalytic reduction of NO_x by CO (CO-SCR) was investigated over metals supported on porous alumina. The Pt, Co, Fe and Ni nanoparticles were dispersed on the alumina and characterized by XRD, textural properties, FTIR spectroscopy, chemical analyses, Py adsorption followed by FTIR measurements, HRTEM and SEM-EDS. Among the solids studied, the Pt/Al_2O_3 and $NiPt/Al_2O_3$ catalysts exhibited improved performance due to the interaction and synergy between the Pt(Ni) nanoparticles and the support. In other words, the electron transfer facility between the PtO_x(Ni) and chlorined Pt species on the support provided a more active solid in the CO-SCR reaction. The surface acidity of Lewis acid sites and the porous features of the Pt/Al_2O_3 and $NiPt/Al_2O_3$ catalysts also contributed significantly to the high performance of these materials in the NO_x conversion. The Pt/Al_2O_3 and $NiPt/Al_2O_3$ catalysts were tolerant to the poisoning by SO_2 and H_2O and depicted a superior catalytic performance, compared to the other solids.

1. Introduction

The impact of the nitrogen oxides, namely NO_x (NO, NO_2, N_2O) on the environment and public health have stimulated the creation of ever more restrictive environmental legislation aimed at controlling the amount of gases emitted by various polluting sources [1–3].

This fact, associated with the need for greenhouse gases abatement (CO, CO_2, hydrocarbons), has driven the search for technologies that allow the reduction of emissions of these pollutants [3–6]. The reduction of NO_x using either the residual hydrocarbons or onboard fuels would be a highly desirable technology [6–10]. In this respect, the selective catalytic reduction (SCR) of NO_x is currently a very effective approach to control NO_x emissions [8–12]. Therefore, various strategies have been extensively used in the NO_x removal through SCR using different reducing agents, e.g., H_2, CO, NH_3, C_3H_6, CH_4N_2O, $C_{10}H_{22}$, C_2H_6O, and C_3H_8 [1–15 (and references herewith)].

Several catalysts have been shown to be active in SCR-NO_x with commercial V_2O_5-WO_3/TiO_2 and V_2O_5-MoO_3/TiO_2 catalysts, being them the most used [11,16,17]. The mechanism of reaction on these commercial catalysts has also been thoroughly investigated [1,18–20]. Although they exhibit high NO_x reduction activity, the commercial catalysts display low resistance to SO_2 and H_2O poisoning. Other disadvantages can be highlighted such as: (i) low operating temperatures (150–250 °C) in reactions involving reduction of NO_x with hydrocarbons HC-SCR) and (ii) narrow operating range (300–400 °C) as in the case of the selective catalytic reduction of NO_x with ammonia (NH_3-SCR) [18]. In addition, the commercial catalysts are susceptible to the poisoning of the active sites by SO_2 and favor the formation of N_2O during long catalytic periods, as well [5,20]. Therefore, the deactivation of catalysts constitutes the main obstacle to the application of SCR technology.

★ This papaer is dedicated to the memory of Prof. Dr. Josue Mendes Filho.

E-mail address: alcineia@ufc.br (A.C. Oliveira)

https://doi.org/10.1016/j.apt.2019.11.003

Regarding the relationship between surface acidity and catalytic performance in SCR reaction, various strategies such as sulfatation of the active sites, introduction of phosphorous, use of acidic supports among others have been employed for promotion of acidity of the catalysts with the consequent improvement of the SCR activity [2,16,17]. However, SCR reaction is inevitably accompanied by catalysts deactivation due to the occurrence of coking and poisoning over acid catalysts with the subsequent decline in the catalytic activity.

To address these issues, improvement of the catalyst properties, engine design and operation conditions have been implemented [5–22]. So far, hydrocarbons, H_2, CO, or even a mixture of H_2/CO have been used as reductant showing benefits during the SCR reactions [1,21,22]. Literature reports show that CO is a typical reductant, which is present in the vehicles exhaust. Besides, the carbon monoxide is widely used in the selective reduction of NO (CO-SCR) over active catalysts in the 260–400 °C temperature range [1,4,18]. Additionally, resistant supports such as Al_2O_3, modified TiO_2, ZrO_2 and zeolites have shown promising during SCR, with Al_2O_3 ones exhibiting a good performance for high temperature SCR reactions [5,9,17]. However, the development of a catalyst with resistance against poisons in SCR reaction is a challenge that has not been accomplished until now.

The present study aims at thoroughly understanding of the role of metal supported on highly porous alumina in the selective catalytic reduction of NO by CO (CO-SCR). The sol-gel-based alumina is widely used as an acid support due to its physicochemical properties in many catalytic processes of industrial importance such as dehydrogenation, oxidations, dehydration and reforming reactions, among others [23–28]. In addition, alumina as a support for SCR reactions has been widely recognized [1,27,28]. In spite of the extensive use of alumina, the findings reveal surprising discrepancies concerning to its catalytic activity in SCR, when using different cations as active sites [1,27].

Herein, we discuss the correlation between surface morphology and catalytic activity for the supported solids during the CO-SCR reaction. The promoted effect of the metals on the relatively low temperature performance of SCR with CO is also investigated.

2. Experimental

2.1. Preparation of the catalysts

2.1.1. Porous alumina synthesis

The alumina support was prepared by sol-gel method [24,29]. Typically, a 103.5 mmol of aluminum tri-sec-butoxide (Al(O-sBu)$_3$, 99% Merck) was dispersed in absolute ethanol (99.5%, Merck). The resulting mixture was thoroughly stirred at 100 °C and then, refluxed for 1 h. Subsequently, 25 mL of a nitric acid solution (0.10 μmol L^{-1}, Merck) was added to the slurry for peptization, and reflux was kept for an additional 14 h. Afterwards, the obtained gel was dried for 2–3 days at room temperature and finally calcined at 700 °C for 6 h under air. The obtained solid was designed as Al_2O_3 support.

Ni supported on Al_2O_3 was prepared by wet-impregnation of the support, using a $Ni(NO_3)_2$ aqueous solution (Vetec). The nominal nickel loading was about 1 wt%. The solid was further calcined at 400 °C under air flow for 2 h and the obtained solid was labelled as Ni/Al_2O_3.

Pt impregnation on Al_2O_3 was accomplished by adding the support into a 1.0 mmol L^{-1} of $H_2PtCl_6{\cdot}6H_2O$ solution (Sigma-Aldrich). The mixture was stirred in a rotatory evaporator during 30 min at 70 °C. The solid was dried and calcined under the abovementioned conditions, having 1 wt% of Pt. The solid was designed as Pt/Al_2O_3.

Other solids were prepared using cobalt and iron nitrates as precursors to produce the Co/Al_2O_3 and Fe/Al_2O_3 catalysts, respectively. For comparison purposes, a solid containing an equimolar amount of Ni and Pt, e.g., 0.5 wt% was prepared similarly to those described above. The solid was labeled as NiPt/Al_2O_3.

2.2. Characterizations

X-ray diffraction (XRD) patterns were recorded on a DMAXB Rigaku diffractometer using CuKα radiation at 40 kV and 25 mA. The scan angle was varied in the 2θ values from 5 to 60° with a step size of 0.02°. Data analysis was done using the JCPDS (Joint Committee of Powder Diffraction Standard).

Nitrogen physisorption isotherms were obtained at liquid nitrogen temperature on an ASAP 2420 apparatus from Micromeritics by nitrogen adsorption at −196 °C. Before the analyses, the samples were heated at 150 °C and outgassed at this temperature for 8 h. The surface area and the pore size distribution were determined by the Brunauer Emmett and Teller (BET) equation and Barrett Joyner Halenda (BJH) model, respectively.

The metal amounts in the solids were determined by inductively coupled plasma optic emission spectroscopy (ICP-OES) with a Varian instrument. Before the analyses, the solids were digested with a mixture of nitric and hydrochloric acid at 90 °C.

Scanning electron microscopy (SEM) images were acquired on a FEI, Quanta 200 FEG electron microscope, which was equipped with an Energy Dispersive Spectroscopy (EDS) system operating at accelerating voltage of 2 kV. Before the measurements, a thin gold film was sprayed on the sample surfaces.

Laser Raman measurements were recorded with a LabRam spectrometer, equipped with a CCD (charge coupled device) with the detector cooled using liquid nitrogen. The excitation source was the 532 nm line with the laser power was 20 mW. The spectral resolution was 4 cm^{-1} using an objective lens of 100 times. The spectra were taken in the 100–2200 cm^{-1} range.

Transmission electron microscopy (TEM) was recorded FEI Tecnai 20 G2 and JEOL JEM-2100 electron microscope at an accelerating voltage of 200 kV. Prior to the measurements, the solids were dispersed in ethanol in an ultrasonic bath and then, deposited on a perforated carbon foil supported by a copper grid.

The Fourier transform infrared spectroscopy (FTIR) spectra of the solids were obtained in a Shimadzu apparatus. The KBr method was used to prepare the samples and the spectra were collected from 400 to 4000 cm^{-1} range.

The type of acid sites was determined through pyridine adsorption measurements followed by FTIR experiments (Py-FTIR) on an 100 FTIR from Perkin Elmer spectrometer, which was coupled to DRIFTS Miracle ATR from Pike Technology (FTIR-ATR). Prior to the measurements, the sample was placed in a furnace under nitrogen flow and heated from room temperature up 350 °C for 1 h. Then, a self-supported pastille (about 15 mg) was pressured to 1 ton cm^2 under a nitrogen flow of 5 cm^3 min^{-1} and placed in an IR homemade cell. Pyridine adsorption was carried out by adsorbing the sonde molecule to the self-supported sample at room temperature for 1 h, accompanied by its desorption at 100 °C for 1 h. At the end of the reaction, a container with a 0.1 mol L^{-1} of hydrochloric acid was placed to remove the excess of pyridine vapors. For each step, the spectra were recorded after evacuating the solids for 1 h at the determined temperature. The spectral resolution was better than 4 cm^{-1} in the range of 4000–600 cm^{-1} with a speed of 20 scan min^{-1}.

2.3. Catalytic activity testing

The selective reduction of NO_x with CO (CO-SCR) was performed in a quartz fixed-bed reactor (inner diameter 0.8 cm) at

atmospheric pressure. Prior to the reaction, the catalyst was pretreated in 80 cm^3 min^{-1} flow of 10% O_2/He at 350 °C for 1 h (heating rate of 10 °C min^{-1}). Then, the solid was purged with helium and finally cooled to 30 °C. The composition of the gases was 500 ppm of NO and 1000 ppm of CO. The mixture was balanced with helium, all gases purchased from White Martins. About 150 mg catalyst (40–60 mesh) was placed into the reactor, where the feed gas passed through the solid at a flow rate of 80 cm^3 min^{-1}. The bed volume was calculated using catalyst bulk density of 0.5 g cm^{-3}. The total flow rate of the reaction mixture was usually 80 cm^3 min^{-1} throughout the catalytic experiments, which corresponds to about a GHSV (gas hourly space velocity) value of 48,600 h^{-1}. The conversions of NO_x and CO were measured by a $NO/NO_2/NO_x$ electrochemical analyzer from Seitron mold chemistry 400. Also, the reaction products were analyzed by using a gas chromatograph (Agilent) with thermal conductivity detector (TCD), respectively.

The poisoning experiments were carried out using 500 ppm of NO, 1000 ppm of CO and balance with He. The mixture of 10 wt% (v/v) of steam and 50 ppm of SO_2 was used as poison during the reaction for 6 h at 300 °C. The GHSV was kept and 48,600 h^{-1}.

The reproducibility of the experiments was tested for two times with using all catalysts. The two experiments resulted in nearly identical average conversions with modest error bars, after two trials of each catalyst, confirming the accuracy of the catalytic results.

The conversions in the CO-SCR reaction were determined at temperatures between 50 and 550 °C.

The conversion of NO_x was estimated by

$$\%X_{NO_x} = \frac{[NO_x]_{in} - [NO_x]_{out}}{[NO_x]_{out}} \times 100 \quad (1)$$

where X_{NOx} represents the NO_x conversion.

The $[NO_x] = [NO] + [NO_2]$ and the subscripts *in* and *out* represent the inlet and outlet concentration of NO_x at steady state, respectively.

The turnover frequency (TOF) was calculated by assuming first-order reaction kinetics and defined as the number of moles of NO_x converted per mole of metal atom per second:

$$TOF = \frac{[NO_x]_{in} - [NO_x]_{out} * F_{gas} * M_{Me}}{m_{cat} * W_{Me} * D} \quad (2)$$

where the $[NO_x]_{in} - [NO_x]_{out}$ represent the NO_x converted; *Fgas*, the molar flow rate; M_{Me}, the atomic weight of the metal (Me); m_{cat}, the mass of catalyst in the reactor bed; W_{Me}, the mass fraction of Me measured by ICP-OES. Moreover, the number of sites dispersed (D) of the samples in TOF calculation was estimated from the surface atomic concentrations.

Calculations of the rate (r) were based on the following equation:

$$r_{NO_x} = \frac{[NO_x]_{in} - [NO_x]_{out}}{W_{cat} * time} \quad (3)$$

where $[NO_x]_{in}$ and $[NO_x]_{out}$ represent the concentration of the gas fed in the reactor and concentration of the gas out of the reactor, respectively. w_{cat} is the catalyst mass per 6 h of reaction time.

3. Results and discussion

3.1. Catalytic performance in the selective catalytic reduction of NO_x by CO (CO-SCR)

Catalyst evaluations in the CO-SCR reaction were carried out in the temperature range of 50–550 °C. The NO_x conversion over the solids is shown in Fig. 1a. Clear differences in activity are seen as a function of the temperature. Below 100 °C, the catalysts display

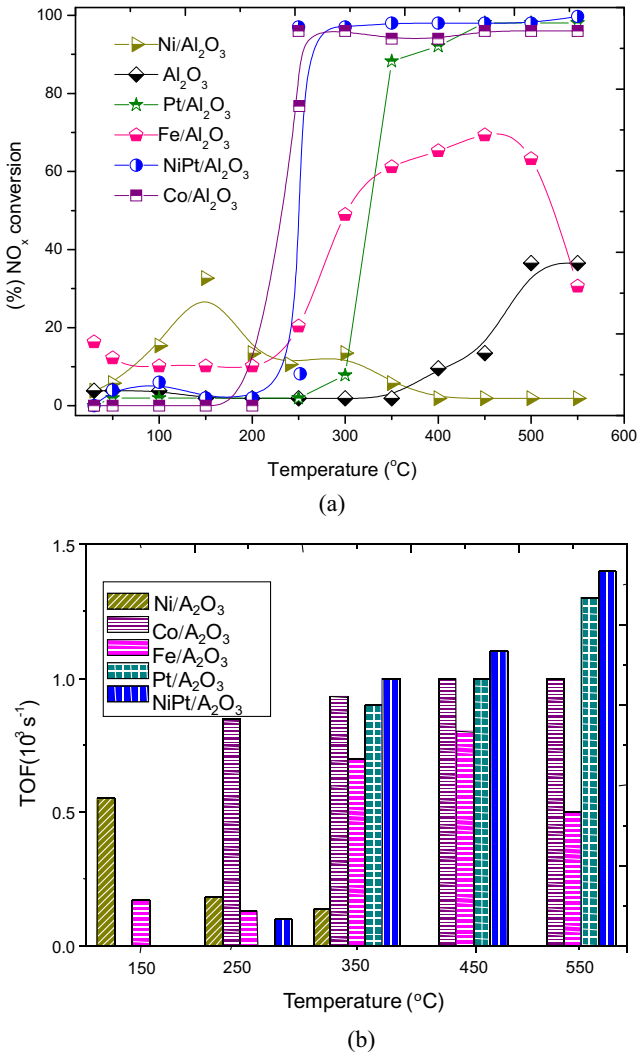

Fig. 1. (a) NO_x conversions as a function of the reaction temperatures for the alumina-based catalysts. (b) TOF as a function of the temperature. Reaction conditions: Reactants composition 500 ppm of NO, 1000 ppm of CO and balance with He.

NO_x conversions lower than 16% because NO_x may be physically adsorbed in the solids at low temperatures and began to desorb with the increasing temperature. Additionally, Al_2O_3, Co/Al_2O_3, Pt/Al_2O_3 and $NiPt/Al_2O_3$ samples are poorly active for CO-SCR reaction (lesser than 3% of NO_x conversions) at 100 °C. It is noteworthy that Ni/Al_2O_3 and Fe/Al_2O_3 exhibit conversions of 16 and 10%, respectively, which is slight higher than the other samples at 100 °C.

The samples begin to differ at temperatures above to 100 °C. For instance, the increase of temperature in the 100–200 °C range results in NO_x conversions for Ni/Al_2O_3 and Fe/Al_2O_3 above to 10%. Meanwhile, the Al_2O_3, Co/Al_2O_3, Pt/Al_2O_3 and $NiPt/Al_2O_3$ catalysts achieve negligible conversions in the aforesaid temperature range. It can be suggested that the elevated textural properties of the Ni/Al_2O_3 and Fe/Al_2O_3 samples may favor the reaction between CO and NO_x. Consequently, the NO_x conversions markedly rise for Ni and Fe active sites from 100 to 200 °C. These results agree well with the findings that indicate the Ni or Fe sites dispersed on mordenite zeolite catalysts show NO_x conversion at low temperatures as low as 250 °C [30].

Further reaction temperature increase from 250 to 550 °C gives different catalytic properties. The conversions over Co/Al_2O_3 and

Fe/Al_2O_3 are above to 13% at 250 °C, in contrast to Al_2O_3, Ni/Al_2O_3, $NiPt/Al_2O_3$ and Pt/Al_2O_3 that have lesser conversions at the referred temperature. Important is to note that Ni/Al_2O_3 exhibits activity only in the 100–300 °C range and then, it fails to null NO_x conversion, even at temperatures approaching 550 °C. Conversely, Pt/Al_2O_3 has an improvement in its performance up to 300 °C where the chlorined PtO_x sites are reduced, as further demonstrated. Also, pure γ-Al_2O_3 sample is solely active at temperatures as high as 400 °C. This is indeed the temperature where the Brønsted acid sites are transformed into the Lewis ones, as shown in aluminum-containing samples [31]. Also, these results are later seen by acidity measurements. The behavior of these samples indicates that the high acidity of the γ-Al_2O_3 itself improves the activity in SCR reaction at high temperatures faster than on Ni/Al_2O_3 possessing lesser acidity than the γ-Al_2O_3.

In the case of Fe/Al_2O_3, an increasing the reaction temperature causes an increment in NO_x conversion to reach a maximum value of 70%; then, the conversion decreases above 450 °C. Taking into account the presence of the α-Fe_2O_3 phase in Fe/Al_2O_3, it can be inferred that such a phase possessing Fe^{3+} Lewis acid sites (latter seen by acidity measurements) may adsorb NO_x already at relatively low temperatures as 250 °C, in line with the findings [5,29]. Also, literature results demonstrate that the thermodynamic equilibrium allows high NO_x conversions to NO_2 by O_2 below 400 °C, although the catalyst is needed to the reaction occurrence [32–34].

Upon using Co/Al_2O_3, the NO_x conversion is very low at 100 °C and then, it approaches the complete conversion rapidly at 300 °C. The SCR reaction studies on Co-based zeolites demonstrate that the Co^{2+} ions are sites more active for such reaction with NO than that octahedrally and tetrahedrally coordinated sites, as in Co_3O_4 phase [33,36]. Presumably, most of the tetrahedrally and octahedrally coordinated Co^{2+} ions from Co_3O_4 phase are located on the alumina surface, as found elsewhere [36]. This suggests that such Co^{3+} ions may be reduced by CO forming CO_2 and Co^{2+} ions with the simultaneous NO_x reduction to N_2, which results in a very rapid activity for the Co/Al_2O_3 catalyst already at 250 °C.

Additionally, the surface acidities of the well dispersed PtO_x and chlorined Pt entities on the alumina give the highest acidity for the former and thereby, resulting in high NO_x conversion within higher temperature region. On the basis CO-TPSR lean trap NO_x measurements for Pt-based samples, the CO reacts with NO_x forming CO_2 and NO simultaneously, along with trace amounts of N_2 above 330 °C [22].

The literature reports that the reaction occurs at a lower temperature, most probably due to the formation of surface isocyanate species (NCO) [7,37,38]. The NCO specie may interact with the Pt and Ni nanoparticles dispersed on the alumina structure already up to 250 °C, as in the case of $NiPt/Al_2O_3$. Moreover, Pt/Al_2O_3 sample possesses Pt^{2+} sites having a redox behavior in the presence of CO, as shown by our previous studies [39]. Besides, the elevated acidity of Pt/Al_2O_3 sample compared with the other samples may be the reason for the high activity of the PtO_x dispersed on the γ-Al_2O_3 sample, most probably due to the NCO formation, as reported elsewhere [22,38].

In other words, adding Pt nanoparticles to the alumina is beneficial to the activity and stability of the catalyst at 300 °C; on the contrary, the synergistic effect between the Ni and Pt on alumina promotes an enhancement of the catalytic properties already at relatively low temperatures as 250 °C. In contrast, NiO sites alone from Ni/Al_2O_3 sample possesses low acidity (further observed by acidity measurements) and thus, the catalyst is not able to convert NO_x at temperatures above 200 °C (Fig. 1a). Indeed, the Ni^{2+} is only reduced above 550 °C [26] and thus, this fact may explain the reasons why the catalytic performance of the solid decay to zero value in the aforesaid temperature.

The general assumptions can be drawn, when considering the abovementioned results. The temperature is one of the main parameters in the CO-SCR process since it can influence the catalytic performance. As found elsewhere, the equilibrium conversion in the absence of catalyst imposes an upper limit of temperature, e.g., >527 °C, having NO_2 conversion of ca. 20% for SCR using CH_4 as reductant gas [40]. The authors demonstrated indeed, that the use of acid zeolites possessing ion-exchanged cations catalysts could promote the formation of a NO_2-binding intermediate resulting in high N_2 selectivity at low temperatures [41]. Thereby, it can be assumed that the minimum temperature of 250 °C is necessary to the complete NO_x conversion to CO_2 and N_2 over Ni/Al_2O_3, $NiPt/Al_2O_3$ and Fe/Al_2O_3. However, the extent of the SCR reaction depends on the presence of the active metal, its acidity and reducibility as well as the structural features of the catalysts.

The number of effective metal atoms exposed on the surface can be estimated by means of TOF as a function of the temperature (Fig. 1b). Generally speaking, the TOF values are in good accordance with the trends of the NO_x conversions. Within the 150–250 °C temperature range, only Co/Al_2O_3, Ni/Al_2O_3, $NiPt/Al_2O_3$ and Fe/Al_2O_3 are actives with Co/Al_2O_3 having the highest TOF value of 0.8×10^{-3} s^{-1} below 250 °C. A further temperature increase to 350–450 °C range gives an increase in the TOF. On the contrary, the TOF is negligible in the aforesaid temperature range for Ni/Al_2O_3 catalyst (Fig. 1b).

At 550 °C, the Pt/Al_2O_3 and $NiPt/Al_2O_3$ catalysts reveal a significant increase in TOF, which suggests that all the surface Pt(Ni) species on the γ-A_2O_3 surface have the same redox ability. At the same reaction temperature, the TOF value for Fe/Al_2O_3 falls to 0.5×10^{-3} s^{-1} and this is an indication of the degradation of the exposed active sites at high temperatures. Interestingly, the Co/Al_2O_3 exhibits a remarkable plateau in the TOF value of ca. 0.9×10^{-3} s^{-1} in the 250–550 °C, which suggests the stability of the exposed Co sites during the reaction.

Considering these results, the α-Fe_2O_3 sites in Fe/Al_2O_3 promotes the reduction of Fe^{3+} Lewis acid sites during SCR in the 250–500 °C interval due to the acidity of the solid and then, its performance experiences a decay owing to the Fe^{3+} reduction to Fe^{2+} and the consequent catalyst phase transformation. This explanation also seems to be consistent with further XRD and FTIR observations on spent Fe/Al_2O_3. Remarkably, the thermal degradation of the Fe/Al_2O_3 at high temperatures may be the leading cause of the solid deactivation. It is worthwhile to note that similar behaviors have been found for Fe dispersed on ZSM-5 at temperatures above to 400 °C [41].

In the case of Co/Al_2O_3 sample, the reaction environment provides the reduction of Co^{3+} species from cobaltite on the defect sites of the alumina, most probably, facilitating the coordination of NO_x or CO molecule to a Co^{2+} Lewis active acid site, as observed elsewhere [30,35,36]. Thereby, the aforesaid Co species improves the catalytic performance at temperatures higher than 250 °C. Consequently, the NO_x conversion exceeds 95% remaining almost constant with additional temperature increase.

Particularly, it seems that the presence of both Pt and Ni nanoparticles on γ-Al_2O_3 has an advantage over using only the Ni ones. Also, these results reveal that the Fe, Co and Pt(Ni) species on alumina provide the catalytic activity of the solids in the CO-SCR reaction at temperatures superior to 250 °C thanks to the unique features of the solids that allows the facile SCR reaction on the solid surface and thereby, exhibiting acid-base and redox abilities. Regarding the performance of the Pt containing solids, e.g., Pt/Al_2O_3 and $NiPt/Al_2O_3$ exhibit much higher NO_x conversions than those of their supported counterparts, which is attributed to the enhanced accessibility of acid sites and Pt(Ni) nanoparticles on the surface of the former solids. The CO is adsorbed on elec-

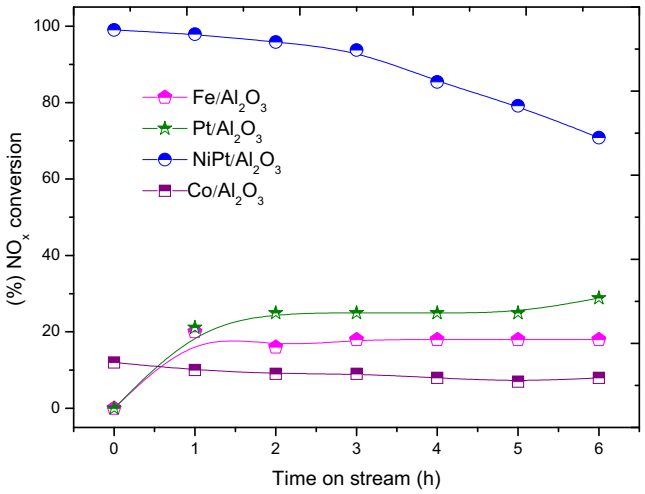

Fig. 2. Time dependence of the NO_x conversion to products over the most active solids. Reaction conditions: Reactants composition 500 ppm of NO, 1000 ppm of CO and balance with He. The mixture of 10 wt% (v/v) of steam and 50 ppm of SO_2 was used as poisons during the reaction for 6 h. The GHSV was kept and 48,600 h^{-1} at 300 °C.

trophilic Pt sites while NO_x is partially reduced forming an intermediate isocyante species and its further decomposition into CO_2 and N_2 at these conditions.

3.1.1. Poisoning of the solids with SO_2 and H_2O

To further investigate the reasons for the deactivation of the most active catalysts, the influence of dual poisoning using H_2O and SO_2 as deactivating agents is studied (Fig. 2). Among the catalysts, the Pt/Al_2O_3, $NiPt/Al_2O_3$, Fe/Al_2O_3 and Co/Al_2O_3 afford the best NO_x conversions and therefore, they are used in the studies at 300 °C.

As seen in Fig. 2, the solids exhibit a NO_x conversion up to 11% at the beginning of the reaction with simultaneous addition of SO_2 and H_2O, except for Pt/Al_2O_3 and Fe/Al_2O_3. As the reaction proceeds, Co/Al_2O_3 conversion remains a plateau in 16% of NO_x conversion while Pt/Al_2O_3 and Fe/Al_2O_3 raise their conversions to values up to 20% within 1 h of time on stream. For $NiPt/Al_2O_3$, a complete conversion is observed initially, and then it falls within 6 h of time on stream.

The literature reports vastly documented the poor tolerance of metal oxides catalysts against sulfur oxides and water vapor during SCR reaction [42,43]. That is to say, the catalyst is poisoned with substantial drop of NO_x conversions nearly to zero at 300 °C. This indicates that the SO_2 and H_2O restrain the NO_x reaction due to the sulfur deposits, especially those bonded to the Fe and Co sites, as in the case of Fe/Al_2O_3 and Co/Al_2O_3 catalysts. The SEM-EDS measurements further confirm these results. Thus, it can be inferred that the adsorption ability of SO_2 on the Co^{3+}/Co^{2+} Lewis and Brønsted sites from Co_3O_4, i.e., formed by water, is much higher than that of NO_x and CO; hence, SO_2 may occupy the Co sites of Co/Al_2O_3 catalyst resulting in low NO_x conversions. Similar effects can be observed for Fe/Al_2O_3, where the Fe^{3+} Lewis and Brønsted sites are poisoned and the catalyst gradually loses its catalytic performance.

It appears that the water vapor initially may reduce (or even to increase) the amount of acidic surface sites and thus, alleviating the deactivation of the Pt/Al_2O_3 and Ni/Al_2O_3 solids. The Pt nanoparticles are likely the active sites for the adsorption of NO_x and CO. Moreover, both Pt/Al_2O_3 and $NiPt/Al_2O_3$ are resistant against water and SO_2 deactivation, under the same conditions during the catalytic runs. Besides, Pt/Al_2O_3 catalyst shows a NO_x conversion of ca. 28%, being constant along of the time on stream. When the $NiPt/Al_2O_3$ is poisoned by SO_2 and water simultaneously at 300 °C, the NO_x conversion of the solid experiences a decline from 100 to 70%, indicating that SO_2 could damage either the Pt or Ni sites of the catalyst and hence, a decrease of the NO_x conversion is seen.

Table 1 shows the intrinsic activity data of the poisoned catalysts. The performances of the solids seem to be negatively affected by the SO_2 and water poisoning. Accordingly, the activity of $NiPt/Al_2O_3$ is 2.7×10^{-10} mol m^{-2} s^{-1}, being the other solids with very low values.

To summarize, the labile SO_2 may react with H_2O to form sulfuric acid steam or even sulfatation of the Ni sites in Ni/Al_2O_3 can occur, probably (later seen by SEM-EDS analyses). Therefore, this kind of vapor may be adsorbed on solid surface blocking the active sites and thus, the adsorption of CO and NO_x is unfavorable. Thus, the SO_2 and water adsorption on Ni/Al_2O_3 may increase and concomitantly deposits sulfur on the solid surface. The low chemical affinity of Ni by sulfur at high temperatures is in agreement with the reference [43]. Contrary to this tendency, the SCR activity of Ni-Mn is favored at high temperatures as high as 360 °C, but the presence of Mn cations is imperative to the better catalytic performance [44]. This can also be related to the coexistence of H_2O and SO_2 with H_2O altering the high amount of Lewis acid sites on $NiPt/Al_2O_3$ and Ni/Al_2O_3. Thus, the SO_2 presence rises the amount of surface hydroxyl Brønsted acid sites of $NiPt/Al_2O_3$, if the solid is sulfated; thus, the aforesaid sites are prone to adsorb SO_2 and thereby, deactivating the solid from 100 to 70%.

Specifically in the case of $NiPt/Al_2O_3$, the simultaneous introduction of SO_2 and water vapor into the reaction system does not cause competitive adsorption between CO and NO_x, although a slight catalysts deactivation is likely. The formation of a dual redox cycle with the participation of NiO and PtO_x species is supposed to play key roles for the superior catalytic NO_x performance on Pt/Al_2O_3 with SO_2 and H_2O resistance.

3.2. Acidity measurements

To classify the fresh catalyst surface acidity, the pyridine is used as a probe molecule followed by Fourier transform infrared spectroscopy (Py-FTIR) measurements. The amount of Brønsted (C_{BAS}) and Lewis (C_{LAS}) are illustrated in Fig. 3. The total acid sites are shown in Table 2.

All solids consisted of low crystallinity materials with γ-Al_2O_3 (JCPDS N° 04-0880), the single phase detected, in accordance with the applied sol-gel methodology [26,30]. The physicochemical characterizations of the fresh solids are shown in the ref.

Table 1
The intrinsic rates (r) of the solids in 6 h of reaction. Textural properties obtained by the nitrogen adsorption-desorption isotherms of the solids in study.

Sample	[a]r × 10^{10} (mol m^{-2} s^{-1})	[a*]S_{BET} (m^2 g^{-1})	[b*]Pore volume (cm^3 g^{-1})
Co/Al_2O_3	0.2	32	0.10
Fe/Al_2O_3	0.2	34	0.10
Pt/Al_2O_3	1.0	56	0.18
Ni/Al_2O_3	–	29	0.08
$NiPt/Al_2O_3$	2.7	43	0.12

[a] The intrinsic rate was obtained by the mol NO_x converted m^{-2} s^{-1} at 300 °C during the SO_2 and water poisoning experiments. Reaction conditions: Reactants composition 500 ppm of NO, 1000 ppm of CO and balance with He. The mixture of 10 wt% (v/v) of steam and 50 ppm of SO_2 were used as poison during the reaction for 6 h. The GHSV was kept and 48,600 h^{-1}.
[a*,b*] The textural parameters of the spent solids.

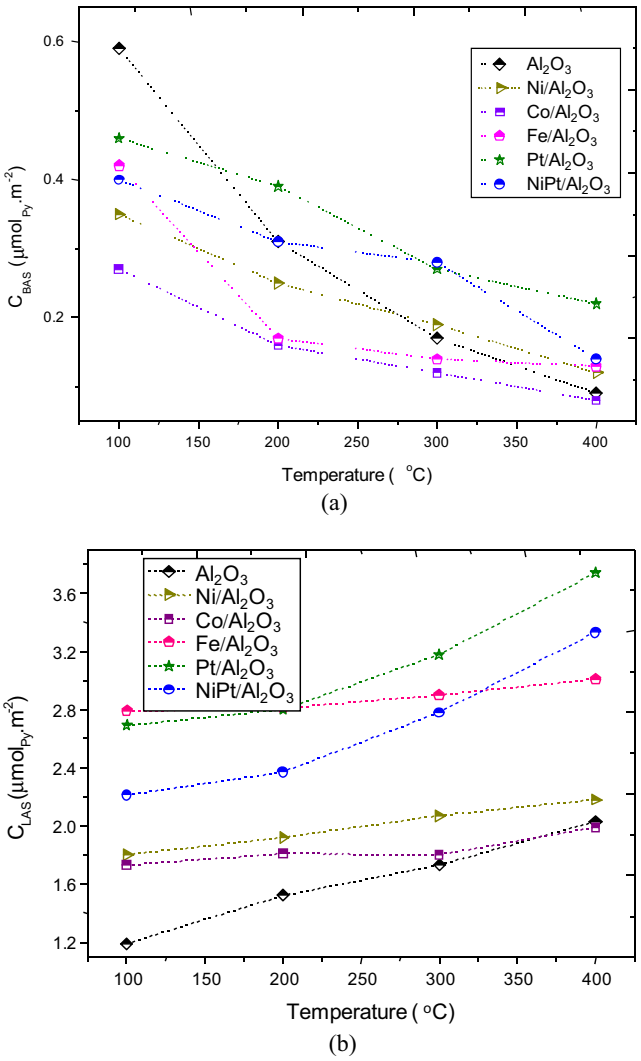

Fig. 3. Acidity of the solids obtained by Py adsorption followed by FTIR measurements. The concentrations of (a) Brønsted (C_{BAS}) and (b) Lewis (C_{LAS}) as a function of the temperature.

[24,26,30]. Moreover, the peaks related to the oxides of Ni, Pt, Co and Fe could be hardly found. This can be attributed to the low the amounts of the metal oxides dispersed on solid surface, as shown by chemical analyses results. Indeed, the amount of metals are close to 1.0 wt% for Ni/Al_2O_3, Fe/Al_2O_3, Pt/Al_2O_3 and Co/Al_2O_3, which is nearly equal to the nominal value. Specifically for $NiPt/Al_2O_3$, the Ni and Pt loadings are 0.5 wt%.

According to the literature, the γ-Al_2O_3 possesses the Lewis acid sites and surface hydroxyl groups with some Brønsted acid sites [45]. Also, pyridine can be adsorbed on alumina, as following: (i) Brønsted acid sites with the characteristic with IR bands at 1540 and 1635 cm^{-1}, (ii) Lewis acid sites with the typical IR bands at 1440–1460, 1575–1580 and 1600–1620 cm^{-1}, and (iii) surface hydroxyl groups with the bands at 1445 and 1596 cm^{-1} [46,47].

Overall, the data in Fig. 3 are taken from the samples with pyridine molecule bonded to the Brønsted acid sites at around 1540 cm^{-1} (C_{BAS}) whereas the pyridinium ions interaction with the Lewis acid sites at about 1445 cm^{-1} (C_{LAS}). Accordingly, the Al_2O_3 sample possesses Brønsted (C_{BAS} is 0.59 μmol_{Py} m^{-2} at 100 °C, Fig. 3a) and Lewis acid sites (C_{LAS} is 1.19 $\mu mol_{Py} m^{-2}$ at 100 °C, Fig. 3b). Also, γ-Al_2O_3 holds the lowest total concentration of these acid sites of ca. 1.78 μmol_{Py} per m^2 (Table 2) confirming that the alumina acidity becomes strong with adding the metals.

Table 2
Total amount of the Brønsted and Lewis acid sites (C_{Total}) taken from the integrated area spectra per BET area. Data were taken from the spectra from 100 to 400 °C.

Catalyst	Temperature (°C)	C_{Total} (μmol_{Py} m^{-2})
Al_2O_3	100	1.78
	200	1.83
	300	1.90
	400	2.10
Ni/Al_2O_3	100	2.15
	200	2.17
	300	2.20
	400	2.30
Co/Al_2O_3	100	2.01
	200	1.97
	300	2.03
	400	2.00
Fe/Al_2O_3	100	3.28
	200	2.98
	300	3.04
	400	3.14
Pt/Al_2O_3	100	3.15
	200	3.19
	300	3.45
	400	3.96
$NiPt/Al_2O_3$	100	2.63
	200	2.68
	300	3.06
	400	3.47

Moreover, the Lewis acidity is dominated at relatively high temperatures as 400 °C. At 200 °C, there are much more Lewis acid sites while the weak Brønsted ones are almost eliminated due to the dehydroxylation of alumina. This is in agreement with the results for pure Al_2O_3 (C_{LAS} = 1.52 μmol_{Py} per m^2), Ni/Al_2O_3 (C_{LAS} = 1.92 μmol_{Py} per m^2) and Pt/Al_2O_3 (C_{LAS} = 2.90 μmol_{Py} per m^2), as observed in Fig. 3b. Moreover, the presence of the same acid sites is seen in the $NiPt/Al_2O_3$, Fe/Al_2O_3 and Co/Al_2O_3 possessing C_{LAS} of 2.37, 2.81 and 1.81 μmol_{Py} per m^2, respectively at 200 °C.

As evidenced by their higher acidities at 300 °C, $NiPt/Al_2O_3$ (C_{Total} is 3.47 μmol_{Py} per m^2) and Pt/Al_2O_3 (3.96 μmol_{Py} per m^2) samples would give the best results in the reaction. These features suggest that the high contributions of Lewis acid sites are at temperatures as high as 300 °C for Pt/Al_2O_3 and $NiPt/Al_2O_3$ besides Fe/Al_2O_3.

The amount of surface acid sites is greatly increased due to the PtO_x and chlorined Pt-based entities on Pt/Al_2O_3 (total acidity of ca. 3.96 μmol_{Py} per m^2) comparing with Ni/Al_2O_3 (total acidity of ca. 2.30 μmol_{Py} per m^2), as demonstrated in Table 2. Moreover, the Lewis acid sites of moderate strength are observed both in low and high temperatures on $NiPt/Al_2O_3$. This might be another important reason why the simultaneous presence of Ni and Pt balances the acidity of the solid with the consequent decline of the stability of the Brønsted acid sites, when comparing Fig. 3a and Fig. 3b.

Similar results are evidenced for Co/Al_2O_3 sample. At low temperatures, the Lewis and Brønsted acid sites are emphasized with a higher number of C_{LAS}, when compared to C_{BAS} in Fig. 3. Interestingly, the total amount of C_{Total} in Co/Al_2O_3 is lower than all solids studied. In agreement, the Co species dispersed in low amounts on γ-Al_2O_3 are not too acidic as compared to Pt and Ni ones [46]. As the desorption temperature increase for more than 100 °C, the results indicate that the surface acidic properties of Co/Al_2O_3 are similar to those of the other samples with a high C_{Total} mainly due to the Lewis acid sites contribution (Table 2). However, this sample shows the lowest amount of C_{Total} values of ca. 2.03 = μmol_{Py} per m^2 at 300 °C.

In the case of Fe/Al_2O_3, the presence of highly acidic Fe^{3+} species provides a higher C_{Total} value of ca. 2.98 = μmol_{Py} per m^2 at 200 °C, as compared to the Co/Al_2O_3 counterpart. When increasing the desorption temperatures at around 400 °C, a significant increase in the Lewis acid sites amount (C_{LAS} 3.14 = μmol_{Py} per m^2) is observed due to the acidic Fe^{3+} surface species formation. As found elsewhere, under SCR conditions, the distribution of isolated Fe^{3+} ions plays an important role during the SCR-NH_3, being the re-oxidation of Fe^{2+}/Fe^{3+} ions the rate-determining step at temperatures below 350 °C ([47–50] and references herewith).

Among the samples studied, the $NiPt/Al_2O_3$ and Pt/Al_2O_3 holding the highest amounts of Lewis acid sites followed by Fe/Al_2O_3 (Fig. 3b). This would improve the catalytic activity of the solids at temperatures superior to 300 °C, as the NO_x conversions greatly increase over $NiPt/Al_2O_3$ and Pt/Al_2O_3 increases in the aforesaid temperature range (Fig. 1b). On the contrary, lower amounts of Lewis acid sites as in the case of Ni/Al_2O_3 and Co/Al_2O_3 (Fig. 3b) may deteriorate the catalytic performance of the solid (Fig. 2). This is expected taking into consideration the deactivation of these solids by coking or oxidation of the active sites, as shown further by spent catalysts characterization.

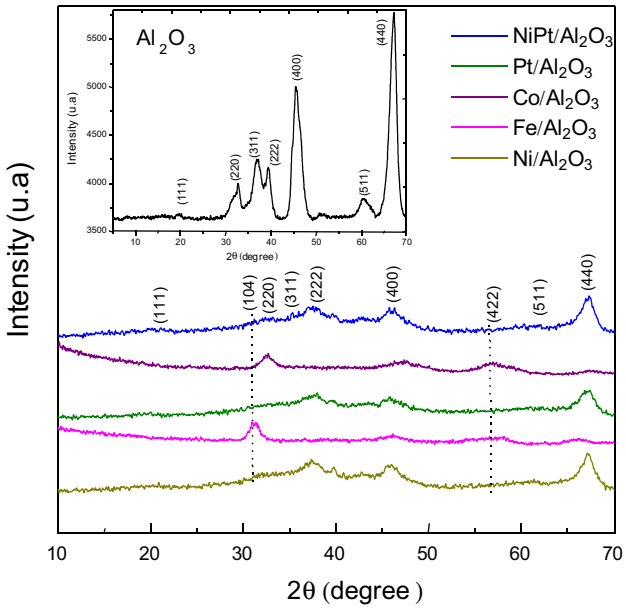

Fig. 4. XRD patterns of the spent catalysts. The included figure is the XRD pattern of bare γ- Al_2O_3. The solids are tested using the reactants composition of 500 ppm of NO, 1000 ppm of CO and balancing with He under distinct at 300 °C. The GHSV is about 48,600 h^{-1}.

3.3. Spent catalysts characterizations

3.3.1. XRD and FTIR investigations

The XRD patterns of the catalysts depict features of semi-crystalline solids. The broad peaks positions specially those at 2θ = 45.8 (4 0 0) and 66.8° (4 4 0) are characteristic of the planes found for γ-Al_2O_3 (space group *Fd-3m*; cubic) [29,49]. Moreover, the $NiPt/Al_2O_3$ and Pt/Al_2O_3 samples exhibit the most γ-Al_2O_3 reflections well resolved, when comparing the pristine γ-Al_2O_3 pattern (included Fig. 4).

This is an indication that the Pt nanoparticles have a homogeneous dispersion on the γ-Al_2O_3 support, as in Pt/Al_2O_3 sample. A similar explanation can be assumed supposing that both Pt and Ni species are well dispersed on γ-Al_2O_3 as in the case of $NiPt/Al_2O_3$; thus, there is no agglomeration of these nanoparticles on solid surface, after the catalytic test. Hence, good performances are shown by the $NiPt/Al_2O_3$ and Pt/Al_2O_3 (Fig. 1a and Fig. 1b). Although the Ni/Al_2O_3 does not evidence significant changes in its structural features, the poor activity of the solid is further explained through the FTIR and SEM-EDS measurements.

On the contrary, the XRD patterns of Fe/Al_2O_3 and Co/Al_2O_3 consist of weak and broader reflections. Some of them, corresponding to γ-Al_2O_3, are vanished from the diffractogram, most probably due to the agglomeration of the Fe and Co particles after the catalytic test. In agreement, the Fe/Al_2O_3 has a peak at 2θ = 31° (1 0 4) that can be indexed to the rhombohedral α-Fe_2O_3 (space group R_3C) [51,52], being superimposed with that of γ-Al_2O_3. Notably, the reflection at around 2θ = 33 (3 1 1) and 56° (4 2 2) matches well with the cubic spinel lattice of Co_3O_4 phase (space group *Fd3m*) [53]. Also, it is reasonable that both Fe and Co nanoparticle sizes are bigger than those found in Ni/Al_2O_3 and Pt/Al_2O_3 solids and thus, providing favorable conditions for the formation of nearly agglomerated particles on former solid surfaces.

The FTIR spectra of the spent solids tested in the CO-SCR are described by an intense absorption band in the 3700–3300 cm^{-1} range (Fig. 5), which is assigned to be from the hydroxyl groups from physisorbed water [22,38]. Obliviously, the bending of the

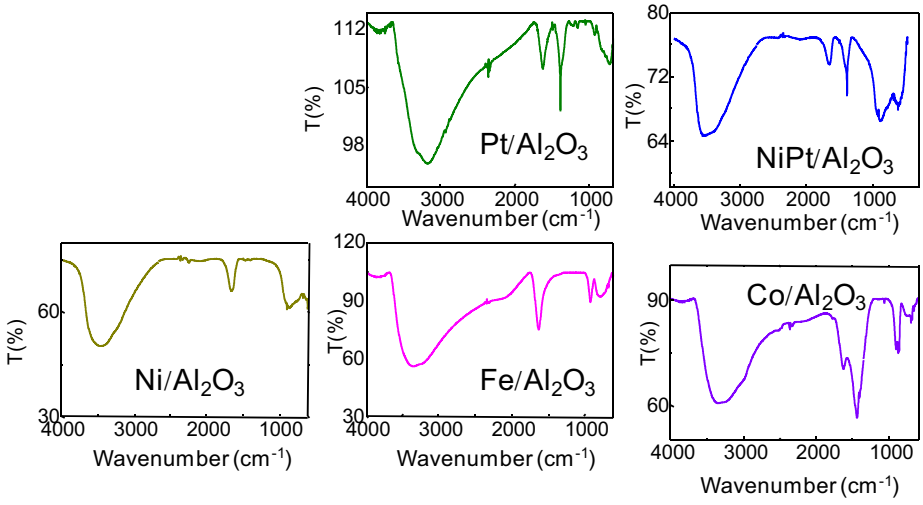

Fig. 5. FTIR spectra of the spent solids tested in the CO-SCR. The solids are tested using the reactants composition of 500 ppm of NO, 1000 ppm of CO and balancing with He under distinct at 300 °C. The GHSV is about 48,600 h^{-1}.

adsorbed water molecules appears at about 1620 cm^{-1}. These bands are found over all solids.

The bidentate nitrates species may appear at about 1585 cm^{-1} as νNO from NO_x decomposition. Notably, carbonates are formed at around 1060, 1377 and 1587 cm^{-1}, which are due to the $\nu_{as}(CO_2^-)$ vibrations, as a result of CO dissociation onto the surface to provide methanation or Water Gas Shift (WGS) reactions. Consequently, the formation of carbon species deposits on Ni/Al_2O_3, Co/Al_2O_3 and Fe/Al_2O_3 spent catalysts is likely. Such reactions are possibly related to the deactivation behavior of these catalysts due to the Ni and Co affinity for CO. In the case of Fe/Al_2O_3, Fe sites suffer from coking and sintering after the catalytic tests, as latter shown by SEM-EDS results.

Moreover, at 1320 and 1420–1000 cm^{-1} ($\nu_{asym}NO_3$), the formation of nitrates species is evident [38,39]. The aforesaid absorption bands are visible mainly on $NiPt/Al_2O_3$ and Pt/Al_2O_3 samples,

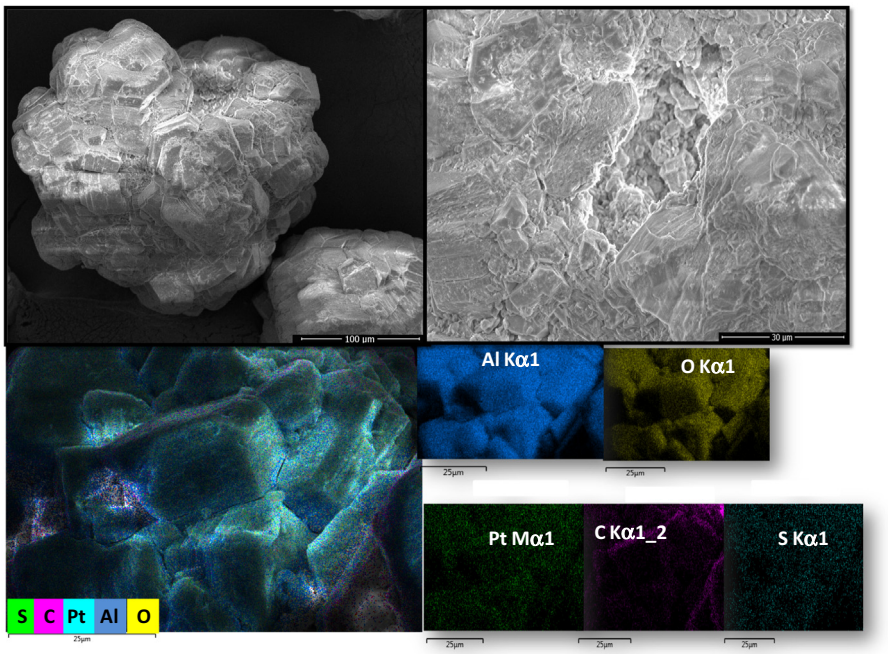

(a)

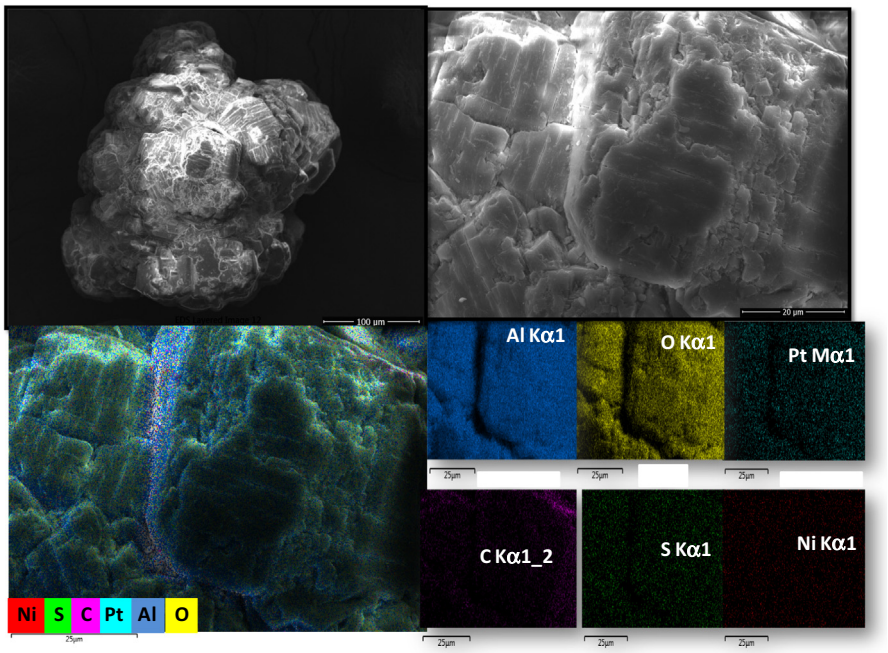

(b)

Fig. 6. SEM-EDS micrographs of the spent solids: (a) PA, (b) NPA, (c) FA, (d) CA and (e) NA samples. The corresponding elemental mapping are also included. The solids are tested in the CO-SCR reaction with the reactants composition of 500 ppm of NO, 1000 ppm of CO and balancing with He under distinct temperatures being 300 °C the maximum temperature that the solid is submitted. The GHSV is about 48,600 h^{-1}. Both SO_2 and H_2O were introduced in the reactor during the reaction for 6 h.

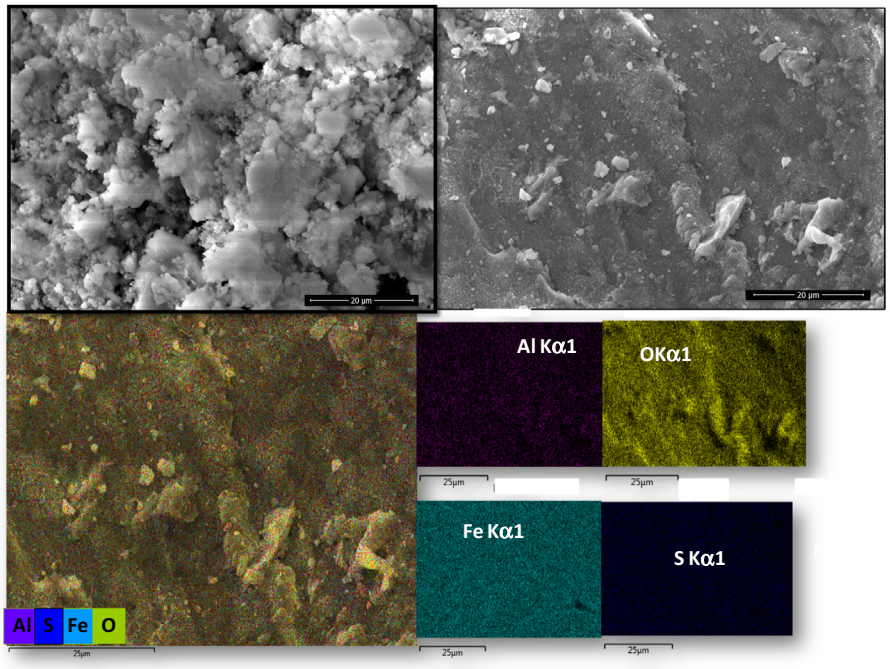

(c)

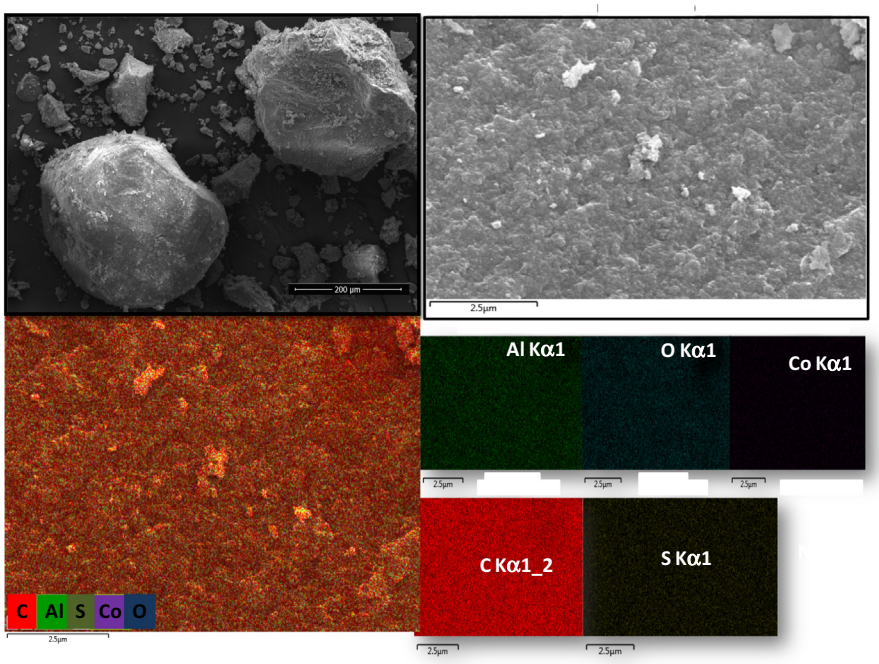

(d)

Fig. 6 (*continued*)

which indicate that the adsorption of NO_x is preferred on the solids. In agreement with our results, the nitrates species are found at about 1418, 1307, 1020 cm^{-1} whereas the chelates are shown at around 1552 cm^{-1}, when adsorbing NO_x at around 350 °C on Pt-based catalysts [38,54,55].

Furthermore, the formate species at about 1350 cm^{-1} arises from the δ (CH) and ν_s (CO^{2-}), as observed in early studies [37,38]. This fact, associated with that the carbonyls species on Pt sites appears in the aforesaid vibration, confirms the formation of the isocyanate formation in the CO-SCR reaction, as found elsewhere [38]. This indicates that the intermediate isocyanate is probably formed due the interaction of CO with NO_x. Also, the carbonyl species is typical of CO interaction with metals such as Pt and Ni [21,38–41]. Moreover, the aliphatic hydrocarbon formation is shown by stretching of ν (CH) confirming that no further oxidation of the CO to heavy coke takes place in the Pt/Al_2O_3 and $NiPt/Al_2O_3$ samples. Thus, the poisoning is inhibited on Pt active sites, which avoids the heavy coking and severe sulfur deposition over the Pt-containing samples. This is consistent with the TEM and SEM-EDS, as discussed later.

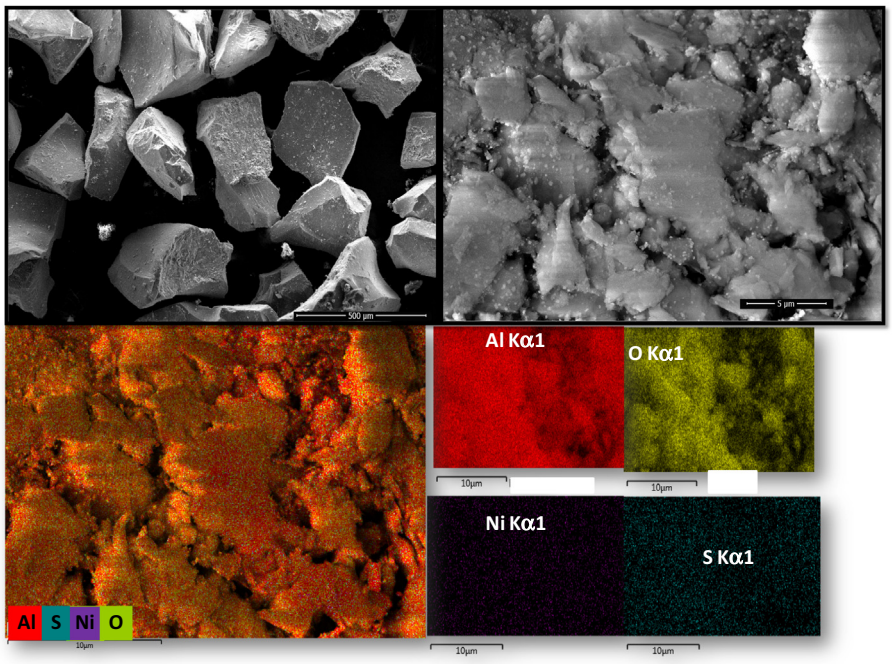

(e)

Fig. 6 (*continued*)

However, the sulfur deposition over the solids (later seen by SEM-EDS results) can not be ruled out. In addition, the catalytic results evidence that the sulfur and water presence do not deactivate severely the Pt/Al_2O_3 and $NiPt/Al_2O_3$ solids, comparing with the Co/Al_2O_3 and Fe/Al_2O_3 counterparts.

3.3.2. Textural properties and SEM-EDS and TEM

The textural properties of the spent solids are obtained through N_2 physisorption analyses at liquid nitrogen temperature. The results are summarized in Table 1. All samples have mesoporous structures, as previously shown by the fresh catalyst characterizations [26,30]. Moreover, the spent solids have a drop in their textural properties, as revealed by the Table 1. This is probably due to the CO-SCR reaction conditions at relatively high temperatures, which results in the sintering and coking of the solids. Amongst them, Co/Al_2O_3, Ni/Al_2O_3 and Fe/Al_2O_3 hold the lowest textural properties due to the agglomeration of their particles on solid surface causing deactivation (Fig. 2), as later confirmed by SEM-EDS measurements. Thus, predominant sintering and coking upon performing the catalytic test are seen on alumina surfaces, which results in lower the textural parameters especially for the Co/Al_2O_3, Ni/Al_2O_3, Fe/Al_2O_3 and Al_2O_3 samples.

On the contrary, Pt/Al_2O_3 and $NiPt/Al_2O_3$ have the opposite behavior. That is to say, either Pt or NiPt nanoparticles dispersed on the samples can effectively convert NO_x into N_2 through the CO-SCR reaction under the same reaction conditions. These samples possessing Lewis acidity, good metal dispersion, unique structural features and redox properties are helpful to protect the surfaces against SO_x and H_2O poisoning and suppress heavy coking.

The morphological features of select spent catalysts are shown by their SEM-EDS and TEM (HRTEM) micrographs. The SEM-EDS micrographs of the samples tested on CO-SCR reaction in the presence of SO_2 and H_2O are shown in Fig. 6.

SEM image of spent Pt/Al_2O_3 shows a dense plate with a rough surface from alumina support (Fig. 6a). This is a result of the sintering of the particles, as seen by the high magnification image; thus, the low textural properties of the spent Pt/Al_2O_3 are a consequence of the sintering effects (Table 1). Pt-containing catalysts are found to be very efficient in SCR only at relatively high temperatures, where N_2O is selectively produced [11]. The behavior of the Pt/Al_2O_3 solid indicates that even upon sintering the solid achieves good levels of NO_x conversion within 6 h of time on stream. However, the support is limited to low resistance against sintering and poisoning by sulfur, as further illustrates by the EDS mappings.

The EDS image depicts a fairly homogeneous dispersion of Pt particles on the γ-Al_2O_3 surface along with C and S elements on solid surface, in accordance with the elemental mapping results. Interestingly, this phenomenon suggests that the harsh reaction conditions that the solid is submitted give simultaneous sintering of the support and coking by sulfur and carbon deposits, owing to the favorable SO_x and CO decomposition on Pt nanoparticles over the highly acid support (acidity measurements). Similarly, the poor performance of Pt/Al_2O_3 catalyst (Fig. 2) may have been partly owing to the higher acidity of the Al_2O_3 support and also owing to larger Pt particles favoring the coking of the solids during the CO-SCR.

The spent $NiPt/Al_2O_3$ catalyst also experiences a slight aggregation of their particles, which are sensitive to S and C deposition, as illustrated by the SEM-EDS image (Fig. 6b). However, no changes in the solid performance are found along of 6 h of reaction. The good dispersion of Pt and Ni active metal sites on alumina in addition to the catalyst relatively lower acidity is paramount to the outstanding performance of the solid under the poisoning conditions studied, as illustrated by the characterization outcomes.

These results confirm the assumptions that the Pt/Al_2O_3 and $NiPt/Al_2O_3$ solids are tolerant against poisoning compared with Ni $/Al_2O_3$, Co $/Al_2O_3$ and Fe/Al_2O_3 due to the CO affinity of the reduced Ni, Co and Fe elements for CO and thus, the latter solids have coking resistance.

In the case of Fe/Al_2O_3, agglomerates of particles are identified after the catalytic test (Fig. 6c), which indicates that the sintering is the leading cause of the deactivation of the solid (Fig. 2). Also, the high magnification SEM image suggests that the aggregates of particles are composed of S element deposited on the solid

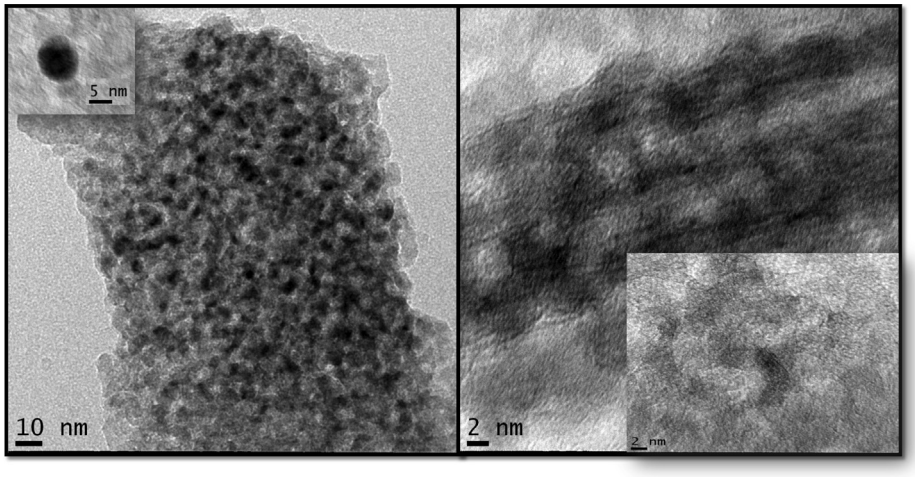

(a)

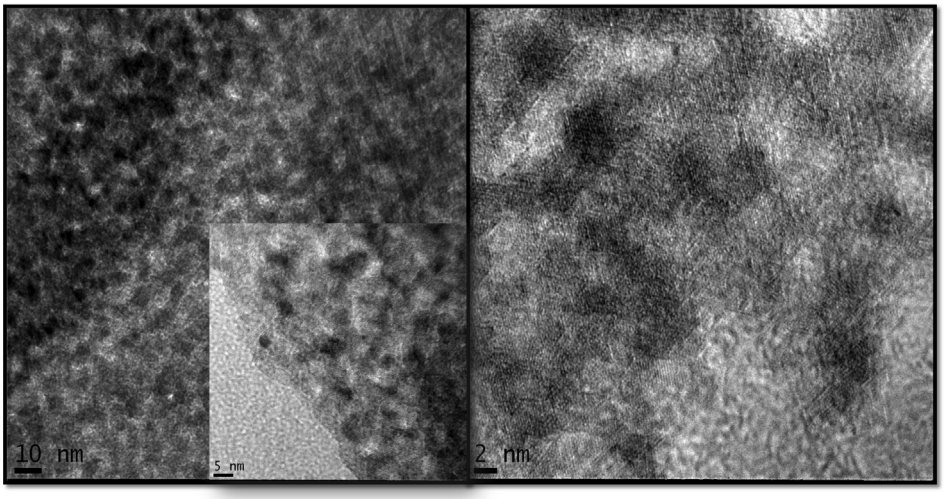

(b)

Fig. 7. HRTEM micrographs of the spent (a) PA and (b) NPA samples. The solids are tested in the SCR-CO reaction at distinct temperatures with the maximum being 300 °C. The reactants composition are 500 ppm of NO, 1000 ppm of CO and balancing with He using the GHSV of 48,600 h^{-1}. Both SO_2 and H_2O were introduced in the reactor during the reaction for 6 h.

surface. Similar results are found for Ni/Al_2O_3 (Fig. 6a). In the case of $CoAl_2O_3$ (Fig. 6d), carbon element is found after the reaction.

$NiPt/Al_2O_3$ and Pt/Al_2O_3 are selected as the most actives catalysts for CO-SCR reaction, thus, a further work is being carried out to find out the reasons for the best catalytic activities of the solids. The TEM images of Pt/Al_2O_3 give evidence that the Pt nanoparticles dispersion remains after the catalytic test, as depicted by the low magnification image in the left of Fig. 7a.

Additionally, based on observations of the HRTEM image in the included Fig. 7a, these particles have sizes in the 0.3–2 nm range. Although these particles are close to each other, no evident sintering of the particles appears to occur after the catalytic test (Fig. 7a, right). Also, sulfur and carbon species are seen (the included Fig. 7a, right) even though the poisoning does not degrade the solid structure. This is consistent with the EDS mapping of Pt/Al_2O_3.

The TEM image of spent $NiPt/Al_2O_3$ shows that small, uneven and random Pt nanoparticles are distributed on the solid surface (Fig. 7b, left). From these data, it can be concluded that the alumina surface indeed is very rich in Pt nanoparticles with sizes close to 1 nm (dark dots in the included Fig. 7b) whereas the Ni ones are not detected (Fig. 7b, right).

Besides, these Pt nanoparticles are resistant against sulfur poisoning, especially those into the alumina pores where almost no heavy carbon is deposited. Thus, the Ni synergistically may act with Pt as active sites, with the former aiding the electron transfer to Pt and subsequently, the electron donation from Pt to the support, thus enhancing the sulfur coking resistance capacity of the $NiPt/Al_2O_3$. This contributes to the good catalytic performance of the solid during the tests with SO_2 and H_2O (Fig. 2).

Evidently, the presence of Ni concomitantly with Pt in $NiPt/Al_2O_3$ improves the catalytic performance; consequently, the severe carbon and sulfur deposition over Ni sites when compared to the analogous Ni/Al_2O_3. The obtained results demonstrated that the Co and Fe give a poor catalytic activity in the SCR process due to their predisposition to the phase transformation and sintering.

The SCR kinetic expressions based on Eley-Rideal and Langmuir-Hinshelwood models for NH_3 as reductant are extensively applied to explain the HC-SCR mechanism [20]. It is expected that Pt^o receives an electron from NO_x (or CO) and the former nitrous gas will be reduced to N_2 and Pt would be oxidized into PtO_x species, in terms of the abovementioned models. In the

current study at 350 °C, however, Pt reduction is not observed over Pt/Al_2O_3 and $NiPt/Al_2O_3$ catalysts in reason of the high temperature required, e.g. >400 °C to obtain metallic Pt on Al_2O_3. Thus, the PtO_x on Al_2O_3 preferentially adsorbs the CO than NO_x in PtO_x sites with the formation of NCO intermediate on the active Pt sites. Further CO_2 oxidation on the metal sites may also occur along with the reduction of the monodentate NO_x adsorbed on the Pt sites to N_2. Afterwards, the PtO_x partially reduced would be restored to PtO_2 by extra oxygen from the Al_2O_3 support and then the next redox cycle starts.

In addition, the Pt reduced state on the Al_2O_3 carrier solely occurs at relatively high temperatures [30]. This is not the case of our samples, in which the partially reduced state of platinum e.g., $(Cl)PtO_x$ is prone to occur promoting the catalytic activity. In this sense, the NO_x species react with CO to form N_2 and CO_2 at short CO-SCR reaction times. As found by TPSR and FTIR experiments, the adsorbed NO_x species decompose to NO, NO_2 and O_2 and simultaneously the NCO/CN (isocyanate/cyanate) species are formed [38]. These species are successively reduced to N_2 and CO_2 through the use of the Pt-containing catalysts at 350 °C with the solids exhibiting NO_x conversion. This may explain the obtained catalytic results for Pt/Al_2O_3 and $NiPt/Al_2O_3$.

4. Conclusions

The NO_x conversions for the Pt-containing alumina samples were higher than those of Ni, Fe and Co supported counterparts. This was attributed to the high acidity of the former samples, confirming that the reaction of NO_x and CO on acidic Pt species enhances the catalytic activity. Adding only Pt to the alumina is beneficial for the stability of the catalyst; on the contrary, the synergistic effect between the bimetallic Ni and Pt on alumina promoted improvement of the catalytic properties only at relatively low temperatures of CO-SCR reaction. The absence of severe sulfur and carbonaceous deposition on the Pt-based solids revealed the high SO_2 and water vapor resistivity of these catalysts.

The acidity, high resistance against poisoning and intimate synergy between the Pt (Ni) nanoparticles and the porous alumina support were considered to be one of the reasons for the superiority of Pt/Al_2O_3 and $NiPt/Al_2O_3$ in the CO-SCR reaction.

Acknowledgment

This research is financially supported by Petrobras ('Física do Petróleo em Meios Porosos' Project Number: F0185).The authors gratefully acknowledge the research funding provided by the CNPq grant nº. 406629/2018-8. M.S. is acknowledged by the support with the experiments. The authors greatly thank to CETENE as well as the Central Analítica da Universidade Federal do Ceará for providing facilities to some measurements.

References

[1] Z. Shang, J. Cao, L. Wang, Y. Guo, G. Lu, Y. Guo, The study of C_3H_8-SCR on Ag/Al_2O_3 catalysts with the presence of CO, Catal. Today 281 (2017) 605–609.
[2] X. Zhang, J. Wang, Z. Song, H. Zhao, Y. Xing, M. Zhao, Ji. Zhao, Z. Ma, P. Zhang, N. Tsubaki, Promotion of surface acidity and surface species of doped Fe and SO_4^{2-} over CeO_2 catalytic for NH_3-SCR reaction, Mol. Catal. 463 (2019) 1–7.
[3] C. Zhang, C. Sun, M. Wu, K. Lu, Optimisation design of SCR mixer for improving deposit performance at low temperatures, Fuel 237 (2019) 465–474.
[4] T. Liu, J. Qian, Y. Yao, Z. Shi, L. Zhang, Research on SCR of NO with CO over the $C_{u0.1}La_{0.1}Ce_{0.8}O$ mixed-oxide catalysts: effect of the grinding, Mol. Catal. 430 (2017) 43–53.
[5] L. Ma, J. Li, R. Ke, L. Fu, Catalytic performance, characterization, and mechanism study of $Fe_2(SO_4)_3/TiO_2$ catalyst for selective catalytic reduction of NO_x by ammonia, J. Phys. Chem. C 115 (2011) 7603–7612.
[6] H. Hamad, T. Hamieh, H. Mahzoul, J. Toufaily, NO_x reduction over MSU molecular sieve catalysts obtained by direct incorporation of platinum and 12-tungstophosphoric Acid $H_3PW_{12}O_{40}$: deNO_x catalysis, Adv. Powder Technol. 19 (2008) 231–252.
[7] M. Seneque, F. Can, D. Duprez, X. Courtois, NO_x selective catalytic reduction (NO_x-SCR) by urea: evidence of the reactivity of HNCO, including a Specific Reaction pathway for NO_x reduction involving NO + NO_2, ACS Catal. 6 (2016) 4064–4067.
[8] T. Liu, Y. Yao, L. Wei, Z. Shi, L. Han, H. Yuan, B. Li, L. Dong, F. Wang, C. Sun, Preparation and evaluation of copper–manganese oxide as a high-efficiency catalyst for CO oxidation and NO reduction by CO, J. Phys. Chem. C 121 (2017) 12757–12770.
[9] G. Xu, Y. Yu, H. He, A low-temperature route triggered by water vapor during the ethanol-SCR of NO_x over Ag/Al_2O_3, ACS Catal. 8 (2018) 2699–2708.
[10] G. Chen, J. Gao, L. Xu, X. Fu, Y. Qin, Optimizing conditions for preparation of MnO_x/RHA catalyst particle for the catalytic oxidation of NO, Adv. Powder Technol. 23 (2012) 256–263.
[11] R. Mrada, A. Aissat, R. Cousina, D. Courcot, S. Siffert, Catalysts for NO_x selective catalytic reduction by hydrocarbons (HC-SCR), Appl. Catal. A: Gen. 504 (2015) 542–548.
[12] K. Tanno, R. Kurose, T. Michioka, H.M.S. Komori, Direct numerical simulation of flow and surface reaction in de-NO_x catalyst, Adv. Powder Technol. 24 (2013) 879–885.
[13] S. Roy, A. Marimuthu, M.S. Hegde, G. Madras, High rates of CO and hydrocarbon oxidation and NO reduction by CO over $Ti_{0.99}Pd_{0.01}O_{1.99}$, Appl. Catal. B: Environm. 73 (2007) 300–310.
[14] S. Roy, B. Viswanath, M.S. Hegde, G. Madras, Low-temperature selective catalytic reduction of NO with NH_3 over $Ti_{0.9}M_{0.1O2-ä}$ (M)Cr, Mn, Fe Co, Cu), J. Phys. Chem. C 112 (2008) 6002–6012.
[15] S. Roy, B.A. Marimuthu, M.S.G. Hegde, Madras High rates of NO and N_2O reduction by CO, CO and hydrocarbon oxidation by O_2 over nano crystalline $Ce_{0.\ 9}8P_{d0.0}2_{O2-ô}$: catalytic and kinetic studies, Appl. Catal. B: Environm. 71 (2007) 23–31.
[16] X. Li, K. Li, Y. Peng, X. Li, Y. Zhang, D. Wang, J. Chen, J. Li, Interaction of phosphorus with a $FeTiO_x$ catalyst for selective catalytic reduction of NO_x with NH_3: Influence on surface acidity and SCR mechanism, Chem. Eng, J. 347 (2018) 173–183.
[17] D. Wang, Y. Peng, Q. Yang, F. Hu, J. Crittenden, NH_3-SCR performance of WO_3 blanketed CeO_2 with different morphology: Balance of surface reducibility and acidity, Catal. Today 332 (2019) 42–48.
[18] X. Sun, R.T. Guo, J. Liu, Z.G. Fu, S. Liu, W. Pan, X. Shi, H. Qin, Z. Wang, X. Liu, The enhanced SCR performance of Mn/TiO_2 catalyst by Mo modification: Identification of the promotion mechanism, Int. J. Hydrogen Eenrgy 43 (2018) 4316038–4316048.
[19] L. Li, W. Tan, X. Wei, Z. Fan, L. Dong, Mo doping as an effective strategy to boost low temperature NH3-SCR performance of CeO_2/TiO_2 catalysts, Catal. Commun. 114 (2018) 10–14.
[20] J.-K. Lai, I.E. Wachs, A perspective on the selective catalytic reduction (SCR) of NO with NH_3 by supported V_2O_5–WO_3/TiO_2 catalysts, ACS Catal. 8 (2018) 6537–6551.
[21] M. Kantcheva, M. Milanova, S. Mametsheripov, In situ FT-IR spectroscopic investigation of gold supported on tungstated zirconia as catalyst for CO-SCR of NO_x, Catal. Today 191 (2012) 12–19.
[22] L. Castoldi, L. Lietti, R. Bonzi, N. Artioli, P. Forzatti, S. Morandi, G. Ghiotti, The NO_x reduction by CO on a $Pt\text{-}K/Al_2O_3$ Lean NO_x Trap Catalyst, J. Phys. Chem. C 115 (2011) 1277–1286.
[23] X. Zhao, L. Mao, G. Dong, Mn-Ce-V-WO_x/TiO_2 SCR catalysts: catalytic activity, stability and interaction among catalytic oxides, Catalysts 8 (2018) 76.
[24] D.C. Carvalho, H.S.A. de Souza, J.M. Filho, A.C. Oliveira, A. Campos, É.R.C. Milet, F.F. de Sousa, E. Padron-Hernandez, A.C. Oliveira, A study on the modification of mesoporous mixed oxides supports for dry reforming of methane by Pt or Ru, Appl. Catal. A: Gen. 473 (2014) 132–145.
[25] A. Khaleel, I. Shehadi, A. Al-Marzouqi, Catalytic conversion of chloromethane to methanol and dimethyl ether over mesoporous γ-alumina, Fuel Process. Technol. 92 (2011) 1783–1789.
[26] H.S.A. de Sousa, F.A.A. Barros, S.J.S. Vasconcelos, J.M. Filho, A.C. Oliveira, Ternary composites for glycerol conversion: The influence of structural and textural properties on catalytic activity, Appl. Catal.A: Gen. 406 (2011) 63–72.
[27] M. Trueba, S.P. Trasatti, γ-Alumina as a support for catalysts: A review of fundamental aspects, Eur. J. Inorg. Chem. (2005) 3393–3403.
[28] M.R. Baiyu, H. Max, K.M. Jr, K. Keyvanloo, T.H. Fletcher, B.F. Woodfield, W.C. Hecker, M.D. Argyle, Effect of different alumina supports on performance of cobalt Fischer-Tropsch catalysts, J. Catal. 539 (2018) 92–100.
[29] J.C.S. Araujo, A.L.G. Pinheiro, M.G.A. Cruz, A.C. Oliveira, J.M.C. Bueno, R.S. Araujo, R. Lang, Catalytic assessment of nanostructured $Pt/xLa_2O_3\text{-}Al_2O_3$ oxides for hydrogen production by dry reforming of methane: Effects of the lanthana content on the catalytic activity, Catal. Today (2018), j.cattod.2018.04.066 (in press).
[30] D. Pietrogiacomia, M.C. Campa, L. Ardemania, M. Occhiuzzi, Operando FTIR study of Fe-MOR, Co-MOR, and Ni-MOR as catalysts for simultaneous abatement of NO_x and N_2O with CH_4 in the presence of O_2. An insight on reaction pathway, Catal Today 336 (2019) 131–138.
[31] A.C. Oliveira, N. Essayem, A. Tuel, J.-M. Clacens, Y.B. Taârit, Structural, acidic and catalytic features of transition metal-containing molecular sieves in the transformation of C_4 hydrocarbon, Appl. Catal. A:Gen. 382 (2010) 10–20.
[32] G.H. Yao, K.-T. Gui, X. Ling, Transport effects and chemical effects on NO removal by SCR, Can. J. Chem. Eng. 96 (2018) 2602–2615.

[33] F. Zhang, S. Zhang, N. Guan, E. Schreier, M. Richter, R. Eckelt, R. Fricke, NO SCR with propane and propene on Co-based alumina catalysts prepared by co-precipitation, Appl. Catal. B: Environm. 73 (2007) 209–219.
[34] K. Ueda, J. Ohyama, A. Satsuma, Investigation of reaction mechanism of $NO-C_3H_6-CO-O_2$ reaction over $NiFe_2O_4$ catalyst, ACS Omega 2 (2017) 3135–3143.
[35] F. Lónyi, H.E. Solt, Z. Pászti, J. Valyon, Mechanism of NO-SCR by methane over Co, H-ZSM-5 and Co, H-mordenite catalysts, Appl. Catal. B: Environ. (2014) 150–151, 218–229.
[36] L.F. Liotta, G. Pantaleo, A. Macaluso, G. Di Carlo, G. Deganello, CoO_x catalysts supported on alumina and alumina-baria: influence of the support on the cobalt species and their activity in NO reduction by C_3H_6 in lean conditions, Appl. Catal. A: Gen. 245 (2003) 167–177.
[37] S.H. Tamm, A. HärelindIngelsten, E.C.Palmqvist On the different roles of isocyanate and cyanide species in propene-SCR over silver/alumina, J. Catal. 255 (2008) 304–312.
[38] I. Nova, L. Lietti, P. Forzatti, F. Frola, F. Prinetto, G. Ghiotti, Reaction Pathways in the Reduction of NO_x Species by CO over $Pt–Ba/Al_2O_3$: Lean NO_x Trap Catalytic Systems, Top. Catal. 274 (2007) 179–184.
[39] J.C.S. Araújo, L.F. Oton, B. Bessa, A.B.S. Neto, A.C. Oliveira, R. Lang, L. Otubo, J.M.C. Bueno, The role of Pt loading on La_2O_3-Al_2O_3 support for methane conversion reactions via partial oxidation and steam reforming, Fuel 254 (2019) 115681.
[40] D.B. Lukyanov, G. Sill, J.L. Ditri, W.K. Hall, Comparison of catalyzed and homogeneous reactions of hydrocarbons for selective catalytic reduction (SCR) of NO_x, J. Catal. 153 (1995) 265–274.
[41] M. Schwidder, M.S. Kumar, K. Klementiev, M. M Pohl, B.A. rückner, W. Grünert, Selective reduction of NO with Fe-ZSM-5 catalysts of low Fe content. Relations between active site structure and catalytic performance, J. Catal. 231 (2005) 314–330.
[42] S. Zhang, B. Zhang, B. Liu, S. Sun, A review of Mn-containing oxide catalysts for low temperature selective catalytic reduction of NO_x with NH_3: reaction mechanism and catalyst deactivation, RSC Adv. 7 (2017) 26226.
[43] L. Zhang, H. Qu, T. Du, W. Ma, Q. Zhong, H_2O and SO_2 tolerance, activity and reaction mechanism of sulfated Ni–Ce–La composite oxide nanocrystals in NH_3-SCR, Chem. Eng. J. 296 (2016) 122–131.
[44] L. Chen, X. Niu, Z. Li, Y. Dong, Z. Zhang, F. Yuan, Y. Zhu, Promoting catalytic performances of Ni-Mn spinel for NH_3 -SCR by treatment with SO_2 and H_2O, Catal. Commun. 85 (2016) 48–51.
[45] J. Zhao, H. Chen, J. Xu, J. Shen, Effect of surface acidic and basic properties of the supported nickel catalysts on the hydrogenation of pyridine to Piperidine, J. Phys. Chem. C 115 (2013) 10573–10580.
[46] S. Haq, D.A. King, Configurational transitions of benzene and pyridine adsorbed on Pt{111} and Cu{110} surfaces: An infrared study, J. Phys. Chem. 100 (1996) 16957–16965.
[47] B.G. Baker, S. Thomson, M. Jasieniak, Cobalt on Tungsten-Modified Alumina Catalysts for Olefin Synthesis M. de Pontes, R.L. Espinoza, C.P. Nicolaides, J.H. Scholz,M.S. Scurrell (Ed.), Natural Gas Conversion IV Studies in Surface Science and Catalysis, vol. 107, p. 9, 1997.
[48] B. Feng, Z. Wang, Y. Sun, C. Zhang, S. Tang, X. Li, X. Huan, Size controlled ZSM-5 on the structure and performance of Fe catalyst in the selective catalytic reduction of NO_x with NH_3, Catal. Commun. 80 (2016) 20–23.
[49] J.V.C. do Carmo, A.C. Oliveira, J.C.S. Araujo, A. Campos, G.C.S. Duarte, Synthesis of highly porous alumina-based oxides with tailored catalytic properties in the esterification of glycerol, J. Mater. Res. 33 (2018) 3625–3633.
[50] S. Brandenberger, O. Kröchera, M. Casapua, A. Tissler, R. Althoff, Hydrothermal deactivation of Fe-ZSM-5 catalysts for the selective catalytic reduction of NO with NH_3, Appl. Catal. B: Environ. 101 (2011) 649–659.
[51] M.G.A. Cruz, F.A.N. Fernandes, A.C. Oliveira, J.M. Filho, A.C. Oliveira, A.F. Campos, E. Padron-Hernandez, E. Rodríguez-Castellón, Effect of the calcination temperatures of the Fe-based catalysts supported on polystyrene mesoporous carbon for FTS Synthesis, Catal. Today 282 (2017) 174–184.
[52] A.P.S. Oliveira, I.S. Gomes, A.C. Oliveira, J.M. Filho, G.D. Saraiva, J.M. Soares, F.F. de Sousa, A. Campos, Styrene oxidation to valuable compounds over nanosized FeCo-based catalysts: effect of the third metal addition, Catalysts 7 (2017) 323.
[53] R. Razzaq, H. Zhu, L. Jiang, U. Muhammad, C. Li, S. Zhang, Catalytic methanation of CO and CO_2 in coke oven gas over $Ni–Co/ZrO_2–CeO_2$, Ind. Eng. Chem. Res. 52 (2013) 2247–2256.
[54] Z. Bian, S. Das, M.H. Wai, P. Hongmanorom, S. Kawi, A review on bimetallic nickel-based catalysts for CO_2 reforming of, ethane, ChemPhysChem 18 (2017) 3117–3134.
[55] F. Prinetto, G. Ghiotti, I. Nova, L. Lietti, E. Tronconi, P. Forzatti, FT-IR and TPD investigation of the NO_x storage properties of BaO/Al_2O_3 and $Pt-BaO/Al_2O_3$ catalysts, J. Phys. Chem. B 105 (2001) 51.